Thermal and nonthermal kinetics of helium monolayers on Pt(111)

T. Niedermayer,[1] H. Schlichting,[1] D. Menzel,[1] S. H. Payne,[2] and H. J. Kreuzer[2]
[1]*Physik-Department E20, Technische Universität München, D-85747 Garching, Germany*
[2]*Department of Physics and Atmospheric Science, Dalhousie University, Halifax, Nova Scotia, Canada B3H 3J5*
(Received 1 February 2004; revised manuscript received 16 August 2004; published 26 January 2005)

Monolayers and submonolayers of helium-4 and helium-3 have been prepared on Pt(111) single-crystal surfaces using a specifically developed ultrahigh vacuum cryostat. Detailed data on thermal desorption and on desorption by absorption of far infrared photons and data on sticking have been obtained; evidence for collision-induced desorption has also been found. With a number of tests we prove that the photoinduced desorption is due to direct coupling of the incoming photons from the blackbody radiation of the environment to the dynamic dipole of the He adsorbate, and not to heating or to nonequilibrium phonon creation, and that this process proceeds independently of the thermal desorption. Theoretical treatments of both thermal and photodesorption are given. The results agree very well with the data in all important aspects; in particular, they reproduce the distinctly different isotope effects in both cases. From the thermal desorption data, we conclude that this system is governed by a two-dimensional gas at low to medium coverages and a compressed phase at high coverages. The thermal kinetics do not exhibit quantum effects, except that present in sticking. The observed photodesorption, however, is a clear quantum effect.

DOI: 10.1103/PhysRevB.71.045427 PACS number(s): 68.43.Mn, 67.70.+n, 68.43.Tj

I. INTRODUCTION

Helium is the smallest and simplest closed-shell atom. Because of its low polarizability, very small van der Waals attractions exist between He atoms and are exerted on it by any medium. In combination with its low mass, this leads to the well-known strong quantum effects in the condensed phases. Also the attractive well in front of a surface is consequently very shallow. Therefore, the main use of helium in surface science is as a probe, for elastic diffraction and inelastic scattering experiments, i.e., as a surface equivalent of neutron scattering. Scattering studies can also be used to derive estimates of the attractive potential for He atoms on a surface, albeit at zero coverage. However, helium adsorption and the formation and properties of mono- and multilayers are also of importance for the basic understanding of the surface interactions of closed-shell systems. The possibility of quantum effects makes it a particularly interesting model system because, on the one hand, its simplicity can provide sensitive tests of theories and, on the other hand, quantum effects can introduce new behavior.

Physisorbed monolayers of helium[1,2] can be prepared only at very low temperatures; they have so far mainly been investigated on high surface area materials like grafoil, using predominantly thermodynamic experiments and evaluation;[3] and on filaments and films with ill-defined surfaces.[4] Direct desorption experiments have so far been reported only for the mentioned films and filaments.[4–7] A quantum desorption effect has been postulated in this latter work in which a single phonon or phonon pulse knocks a He atom off the surface;[5–7] this interpretation has been challenged.[1] We do not know of any work on helium (sub)monolayers on macroscopic single crystals as used in most surface science experiments, nor with the usual arsenal of methods from this field.

In a continued effort to carefully characterize physisorption, the Munich group has investigated experimentally the adsorption/desorption kinetics of all rare gases, neon through xenon, on the close-packed Ru(001), H/Ru(001), and Pt(111) surfaces, and of molecular H_2 and D_2 on H/Ru(001), using mainly high-precision, wide range, temperature-programmed desorption (TPD),[8] from which the energetics and dynamics of these layers have been derived.[8–10] We have shown that the dynamics is influenced by a quantum effect in sticking, not only for the light atoms but to at least argon;[11,12] that another quantum effect becomes apparent for molecular hydrogen in compressed monolayers;[9] and that the thermodynamics of the layers, including ordered phases and two-dimensional (2D) phase coexistence, can be well observed in such experiments.[8,13] The theoretical models developed by the Halifax group[14] were very important for this success.

Because of the experimental difficulties at very low temperatures, we had previously not been able to extend our methods to the helium isotopes, even though very interesting information was to be expected. We have now been able to carry out such work; the results are reported here. We will show that here, as well, the thermodynamics and dynamics of the helium adsorbate show up in the desorption experiments. In addition, we report a very interesting desorption effect induced by thermal radiation of the surroundings. Detailed tests show this to be due to coupling of a *photon* to the surface complex (helium plus modified surface), leading to direct nonthermal photodesorption, not to heating or to creation of a nonthermal *phonon* pulse. Thus this is quantum desorption induced by a different mechanism than the quantum (phonon-mediated) desorption mentioned above. Its theoretical treatment, as given below, draws on previous work on photodesorption theory by the Halifax group.[15,16] Similar effects have been predicted[17] and reported (see Ref. 18 and references therein) before for molecular hydrogen; no experiments for helium have been carried out to date. A short report on our work has appeared.[19]

The aim of our work was to not only obtain clear experimental facts, but apply to them appropriate theoretical mod-

els, the goal being an improved physical insight into the mechanisms governing the observed effects, with good agreement between important predictions of the models and experimental data. As we will demonstrate below, this goal has been reached: we not only recover the main dependences of thermal and photodesorption on isotope mass, coverage, and temperatures of radiation and sample, but we can quantitatively reproduce the magnitudes of the observations. We therefore believe that our interpretation of the effects is physically reliable.

This paper is structured as follows. We first give a description of the experimental developments and apparatus which enabled us to successfully carry out the experiments. Then we give an account of the main experimental data and the qualitative conclusions to be drawn from them. After a description of the theoretical models which we use for the detailed interpretation, we apply these and show how they can explain the data. The main conclusions are collected in a summary.

II. EXPERIMENT: APPARATUS AND PROCEDURES

Our general approach in getting thermodynamic and dynamic information on adsorption layers by precision TPD[8] requires the sample to be coolable to a temperature at which the adsorption layer is essentially irreversibly adsorbed (thermal lifetime more than 10^6 s), to be heatable in a well-programmed way with linear heating rates between 0.01 and 5 K/s, and to be quickly heatable to high temperatures *in situ* for cleaning, with a rapid return to the base temperature to keep the sample clean, all this at base pressures at least in the low 10^{-11} mbar range. As the temperature expected for irreversible adsorption of helium to occur on a transition metal surface is below 3 K, our previously developed techniques[20] for cooling well-defined single crystals in a normal ultrahigh vacuum apparatus were not sufficient [lowest sample temperature reached was 4.8 K (Ref. 9)] and had to be extended. A mere lowering of the cryostat temperature would not suffice, since the requirements contradict each other—low base temperature and fast cooldown require strong coupling of the sample to the cryostat, high heating for cleaning the opposite; exact programmed heating for TPD runs is intermediate. With a specially developed cryostat[21] in a conventional ultrahigh vacuum system (base pressure 3×10^{-11} mbar), we succeeded in reaching a sample base temperature of 2.3 K, while maintaining the ability for fast heating and cooling to/from high temperatures, as well as for slow heating with precise heating rates in a small range above the base temperature. This was accomplished by a transfer tube supplying a continuous He gas-liquid mixture, carefully optimized for constant flow which was mandatory for a stable base temperature. At its end, gas and liquid are separated and the latter fed into a two-stage expansion cryostat, in which both stages are pumped. In the first stage about 25 mbar, corresponding to 1.9 K, is reached; a small reservoir of about 200 ml liquid helium together with connecting tubes damp possible pressure oscillations. The second stage is contained in the cooling head made of silver; in it a pressure of about 2.9 mbar, corresponding to 1.4 K, is reached. It contains only a few milliliters of liquid, so that helium loss is minimized during heating of the sample. The conflict in the coupling requirements between head and sample was solved by connecting them via a heat switch which makes or breaks the connection from cryostat to crystal by means of a pressurizable bellows (He gas at 3 bar above ambient) acting against disk springs. When closed (bellows evacuated), the springs press the sample, which is mounted in a frame, against the cryostat head with a force of about 200 N.[21] Rapid heating to 1000 K for cleaning purposes while disconnected, followed by fast cool-down after reconnection to keep the sample clean, were thus possible.[22] Carefully optimized connections between crystal and cooling head led to a stable temperature of 2.3 K at the sample, when connected to the head by the heat switch. The very important calibration of the thermocouples used for measurement and control of the sample temperature, T_s, during TPD was again accomplished[20] by comparison with the thermal desorption traces of multilayers of condensed gases, which can be directly related to their equilibrium vapor pressure. Our previous calibrations had reached 4.8 K by using multilayer desorption of Ne and D_2.[20] To extend it to lower temperatures, H_2 multilayers served for the most important comparison since their desorption range overlaps well with that of helium monolayers (see Fig. 1) down to about 3 K. Below 3 K, we extrapolated the calibration curve according to the thermocouple data; several tests[21] as well as the consistency of the data derived (see below) show that this cannot be off the exact behavior by much. We mention that the absolute error to be given below for desorption energies largely stems from the uncertainty in the literature values of the heats of evaporation of hydrogen which show discrepancies up to 20% (see Ref. 21 for details). The programmed sample temperatures for TPD were produced by electron bombardment from a shielded filament behind the sample, regulated by a special, purpose-built, electronic regulator; this made linear heating rates between 0.01 and 5 K/s in the range 2.3–20 K possible. The high cleaning temperatures of around 1000 K

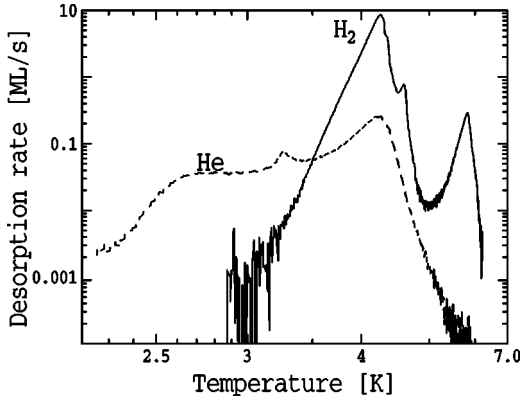

FIG. 1. Calibration of sample temperature during heating below 5 K by measurement of the evaporation curve for hydrogen multilayers (rate in monolayers/s on log scale vs inverse temperature, running from right to left) which is equivalent to the vapor pressure curve (Ref. 20). The TPD curve for a ^{4}He monolayer (heating rate 0.2 K/s) is shown to the same scales. Good calibration confidence in the range 3–4.3 K is obtained.

were also attained by electron bombardment, with the heat switch open. TPD spectra, for determination of both sticking coefficients and desorption rates, were acquired with a mass spectrometer in a "Feulner cap" arrangement.[23] This leads to relatively large pressure increases upon desorption which are directly proportional to the desorption rate if appropriately corrected for small background effects.[8,21] While desorption is carried out, the cap, the front of which is placed at a small distance (0.13 mm, accurately set by capacitance measurement) from the sample surface, covers the full solid angle seen by the surface. In the initial setup, the cap was at room temperature (RT, about 295 K). When nonthermal desorption turned out to be appreciable under these conditions (see below), the cap temperature—and thus the radiation temperature seen by the sample—was made variable between 90 and 470 K.

A Pt(111) crystal was chosen as the sample because its preparation as well as rare-gas adsorption on it are well known and documented.[9,10,13] Its surface was prepared and characterized with standard procedures for cleanliness and low defect content.[10] It could be covered with helium either by admitting gas into the system (gas at 300 K), or through a multicapillary doser (also T_g=300 K, but incoming angle limited to about 20 deg around the surface normal), or through the variable temperature cap (T_g correspondingly lower); the various characteristics will be discussed more fully below when reporting the sticking coefficients. TPD spectra over more than three orders of magnitude in the rate were sufficiently reproducible that the rate could be calibrated in monolayers per second by reference to the saturated monolayer (see below). Both ^{4}He and ^{3}He mono- and submonolayers were investigated. Multilayer formation does not occur at 2.3 K because of the weak He—He interaction and the low pressures used. As will be seen from the results below, the ratio of binding energies of the first to higher monolayers on Pt(111) is of the order of 8. This constitutes an anomaly compared to all other rare gases on Pt(111) for which this ratio is between 1.5 and 1.8.[10]

III. EXPERIMENTAL RESULTS

A. Main characteristics: Thermal and photodesorption

In the initial stages of this work, both the dosing gas and the environment seen by the sample were at room temperature (about 295–300 K). After saturating the surface with ^{4}He at the base temperature, a relatively small, unstructured desorption peak between 3.5 and 4 K was obtained in TPD (Fig. 2, range A), and below the peak a desorption signal was seen which slowly decreased during heating (range C). This latter prepeak signal was distinctly larger for ^{3}He (Fig. 3), and decreased faster. Tests showed that the decline of the prepeak signal was *not* connected to the (increasing) temperature, but to *time elapsed* after dosing (see below). Increasing the heating rate from 0.03 to 0.2 K/s does not affect the prepeak desorption rate significantly but reduces the time before the thermal desorption range is reached, i.e., the amount desorbed in the prepeak region. As a result, the thermal peak increases. Cooling the cap, i.e., lowering the radiation temperature seen by the surface, to 90 K reduces the

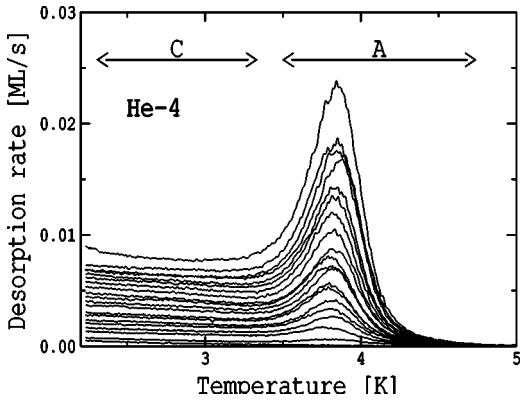

FIG. 2. TPD curves for ^{4}He from submonolayers up to the maximum coverage obtainable at gas and radiation temperatures of 295 to 300 K [about 0.84 ML (Ref. 24)]. The ranges of thermal desorption (A) and photodesorption (C) are indicated. Heating rate: 0.03 K/s.

prepeak signal drastically for low initial coverages, and increases the total amount desorbed in the thermal peak (peak integral) by about 20% or more. Furthermore, for coverages approaching saturation under these conditions, structure is introduced in the desorption spectra which is reminiscent of the "compression peaks" well known from other rare-gas systems,[8,13] for both isotopes (Figs. 4 and 5).

It was suggestive that part of the lower saturation coverage with RT environment and gas, as compared to cold gas, stemmed from collisional desorption, i.e., energetic He atoms in the thermal distribution at RT knocking off adsorbed atoms, so that a lower maximum steady-state coverage was obtained before the start of desorption. Indeed, this could be corroborated by decreasing the He gas temperature and by using other layers, e.g., neon, which also was susceptible to this effect; these results will be reported separately.[25] However the slow prepeak desorption seen in the TPD traces below 3 K cannot be caused in this way, because no He atoms collide with the surface under TPD conditions. Varying the time between exposure of the surface and start of the heating procedure, or following the desorption signal with time at constant temperature in the range well below the thermal desorption peak, showed that the *entire* coverage

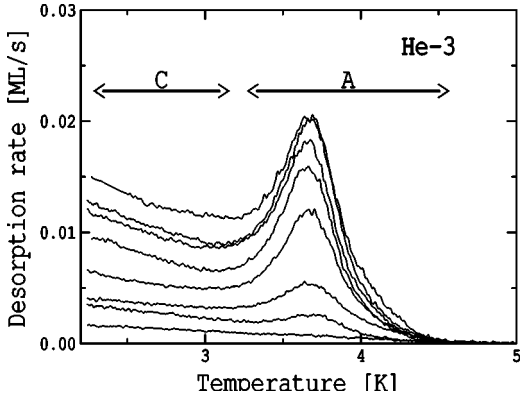

FIG. 3. Same as Fig. 2, but for ^{3}He submonolayers. Maximum coverage 0.82 ML (Ref. 24).

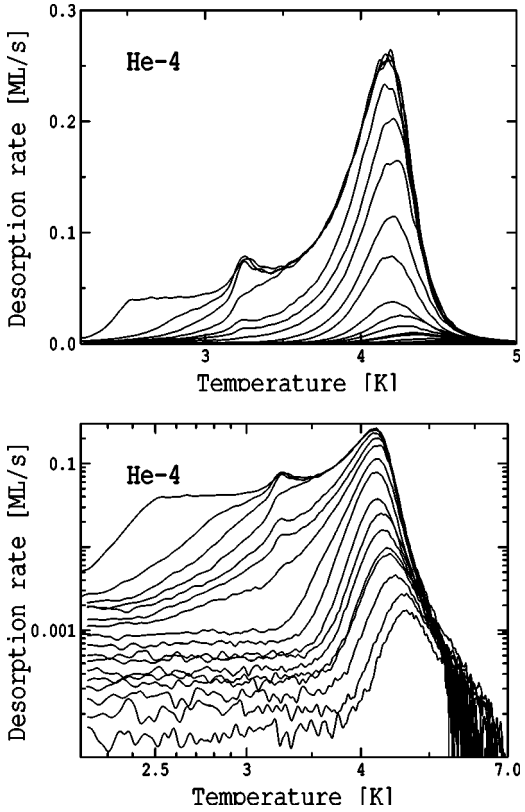

FIG. 4. TPD curves for ^{4}He up to monolayer saturation, obtained by adsorption at radiation and gas temperatures of 90 K (photodesorption minimized). The compression phase (plateau plus peak below 3.5 K) is obvious. Heating rate: 0.2 K/s. Top panel: Linear plot. Bottom panel: Quasi-Arrhenius plot [log(rate) vs $-1/T$] which linearizes the exponential T dependence, emphasizes the range of small rates, and shows the small but definite contribution of photodesorption.

was susceptible to this slow desorption; the desorption proceeded proportionally to the coverage to a good approximation, yielding a first-order desorption rate constant of about 0.01 s^{-1} for ^{4}He at 2.3 K and RT environment. In Fig. 6, a sequence of such isothermal desorption runs is shown for ^{4}He at successively higher sample temperatures, T_s, up to 3.5 K and replotted as rate versus coverage (desorption runs from right to left). Small deviations from first order and a very small but systematic increase of the rate (by about 10% from 2.3 to 3.0 K) can be seen. Only when the temperature is increased into the foot of the thermal peak (topmost lines) does a brief thermal desorption spike occur, which increases if T_s is further increased (not shown); subsequently the nonthermal process runs again. For ^{3}He, similar data with about 50% higher rates have been obtained, consistent with the higher photodesorption effect seen in the TPD traces (Fig. 3). The approach to zero rate at zero coverage can be clearly seen, which proves that the complete layer is subject to this nonthermal mechanism.

When the radiation temperature, T_r, of the environment seen by the surface was changed by cooling the cap, the photodesorption effect became smaller [Fig. 7 (top)]; heating the cap increased it. At $T_r=90$ K, the rate constant was five to six times smaller compared to RT, for ^{4}He (by a factor 4

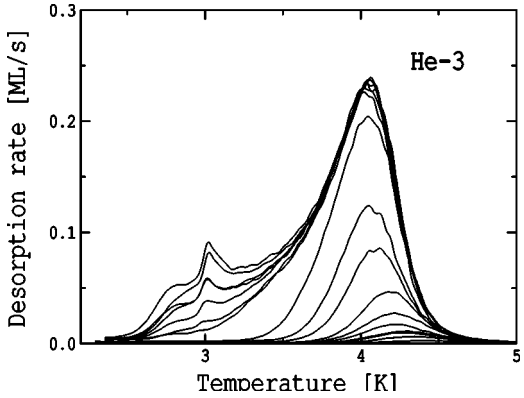

FIG. 5. Same as Fig. 4 top, for ^{3}He layers.

for ^{3}He). Isothermal desorption is considerably faster for the *compressed* layer formed by saturation with gas from a 90 K environment, as can be seen in Fig. 7 (bottom): if roughly interpreted as a first-order process, the desorption rate constant in the compression range is about eight times higher at $T_r=180$ K, and more than 40 times for $T_r=300$ K. However, the high rates at high coverages certainly contain strong contributions from thermal desorption which here cannot be unequivocally separated from photodesorption purely on the basis of experiment; we will return to this question in the discussion.

By varying the cap temperature, we measured the dependence of the rate on the radiation temperature. Figure 8 shows considerable scatter of the results which is due to changes of the general background in the system when the temperature of the large cap is changed; this is particularly severe when the cap was heated ($T_r=400$ K). However, it can be seen that the dependence is best compatible with a roughly linear dependence and certainly not a T^4 relation, as would be expected if a surface heating effect were responsible. Irradiation of the sample with a halogen lamp directed at the surface increased the photodesorption dramatically, ir-

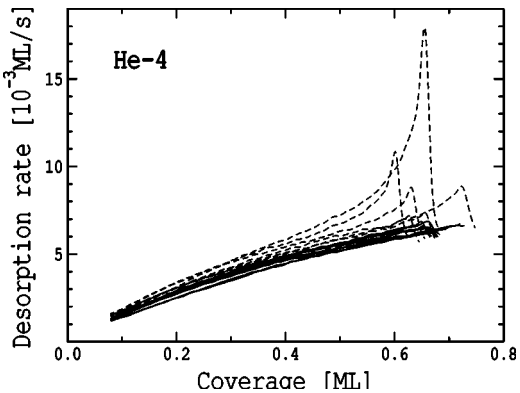

FIG. 6. Isothermal desorption runs for ^{4}He for room-temperature surroundings ($T_r=300$ K), each starting at around 0.7 ML, at constant sample temperatures, T_s, in 0.1 K steps from 2.3 to 3.0 K (solid curves; photodesorption only), and from 3.1 to 3.5 K (dashed curves; initial thermal desorption spikes increasing with T_s). The small increases of photodesorption rate are systematic with T_s. Desorption runs from right to left.

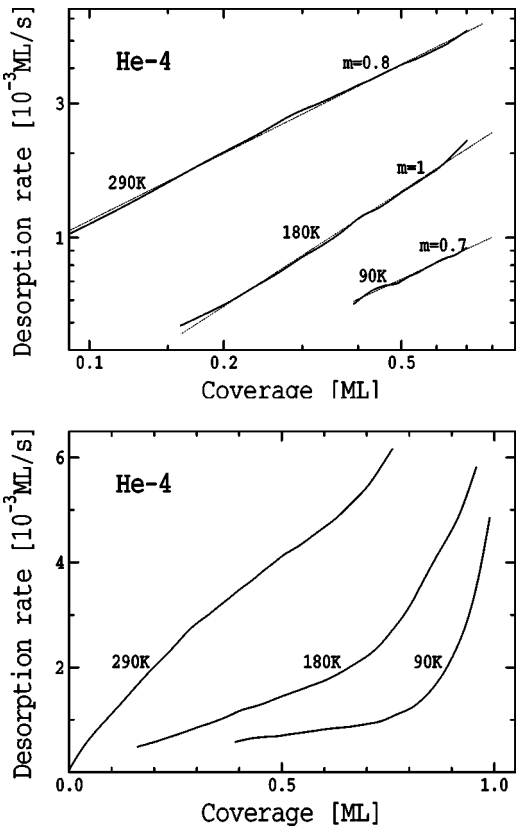

FIG. 7. Isothermal desorption for ^{4}He at T_S=2.3 K, for the radiation temperatures indicated. Curves run from right to left. Top: starting at 0.7 ML; straight lines are fits to the apparent order of desorption, *m*. The effect is pure photodesorption. Bottom: starting at the respective saturation coverages indicated. The strong rate increase in the compression range is obvious; it contains considerable contributions from thermal desorption.

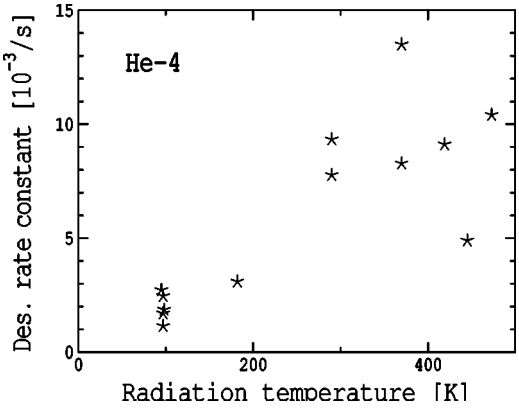

FIG. 8. Photodesorption rate constant in the low coverage range (below 0.65 ML) for He-4, as a function of radiation temperature of the surroundings.

respective of sample temperature, even though the latter increased by less than 0.2 K (from 2.3 to 2.5 K) at maximum intensity. Unfortunately irradiation by a monochromatic IR source in a controlled way could not be performed in our setup. Heat conduction calculations[21] corroborate that the sample temperature increases so little under our conditions that thermal effects can be excluded except very close to incipient thermal desorption. On the other hand, comparing TPD traces for medium to low initial coverages obtained with T_r of about 300 K and 90 K showed them to agree well, if for the former the nonthermal effect as determined separately (see above) was subtracted. For some further tests, see Ref. 21.

These results show clearly that (i) the normal thermal desorption (above 3 K for coverages up to 0.7 ML) and the nonthermal, photoinduced effect are independent and additive; and that (ii) the photoinduced effect is *not* caused by heating but by photon absorption. Because of (i) we can therefore analyze the two effects separately. As to the photoinduced desorption, it is clearly a nonequilibrium, quantum effect. Interestingly, we found that H_2 and D_2 monolayers on Pt(111) also show this photoinduced desorption, albeit much more weakly; in this case, mono- and multilayers could be compared, and the effect was clearly weaker for multilayers, corroborating the participation of metal excitations (see below). No effect was seen for Ne or more strongly bound atoms. Without further analysis one could argue for either a mechanism via nonequilibrium phonons,[7] or for direct absorption of a photon in the adsorption complex and conversion of its energy into desorption of a helium atom.[17]. As we will show in Sec. IV, the latter mechanism is the correct one. The observed isotope effect will be a decisive argument; it can even be used in a qualitative way. If a single nonequilibrium phonon or a nonequilibrium phonon pulse would knock off a helium atom, then the efficiency for ^{3}He should be *smaller* than that for ^{4}He, because sticking—the reverse of desorption—is less efficient for the lower mass, all other parameters being equal.[12] This is in qualitative disagreement with our results. In the theory section, we will show that not only the correct qualitative isotope effect, but even quantitative agreement is found for direct photoabsorption into the adsorption complex.

B. Thermal desorption

For the spectra from (sub)monolayers produced and desorbed with 90 K gas and surroundings, the photoinduced contribution is small and the TPD spectra can be interpreted in the standard manner, as phonon-mediated thermal desorption. Qualitatively it is obvious from the sequence of TPD peaks that in the range of the single structureless peak, up to about 70% of the maximum coverage attainable, the layer is a two-dimensional gas. This can be concluded from the close to first-order behavior of the peak shape with coverage, which only shows a small downshift of the peak temperature with increasing initial coverage. In particular, the absence of a common leading edge to the spectra proves that in this system, *no* phase equilibrium exists between a 2D condensate and a 2D gas. This is contrary to most other rare-gas systems on transition metal surfaces, where the common leading edge has been observed.[8–10,13] Furthermore, the close similarity of the TPD peaks of ^{4}He and ^{3}He, which exhibit only a small relative shift in temperature, proves clearly that no quantum effect is present in the two (sub)monolayers under our conditions, i.e., above 2.3 K. Above 0.7 of saturation,

the development of a new peak which sits on a broad shoulder suggests the formation of a new phase. We will discuss its properties in Sec. IV. Here also, no basic difference exists between the two isotopes.

As to quantitative analysis of the TPD traces, we have carried out various evaluations (rising edge analysis, heating rate variation, isosteric evaluation, peak fitting).[8] We have found that, even in the single peak range, the parameters determined vary by about ±10%, depending on the analysis chosen. In each method, different errors contribute: in leading edge analysis, the background due to the photodesorption, even for 90 K surroundings where this effect is small, is not well known, but has a strong influence on accuracy; in isosteric evaluation, the uncertainty in the trailing edge, due to the general background subtraction,[8] introduces uncertainties; and in peak fitting, a range of correlated energy/preexponential pairs can fit the data about equally well. We find desorption energies between 90 and 120 K correlated with compensating first-order preexponentials between 10^9 and 10^{12} s^{-1}, for both isotopes, in the single peak range. For equal preexponentials, the desorption energy for ^{3}He is about 3–4 % smaller than that for ^{4}He, corresponding to the difference of peak temperatures of about 0.2 K. If we assume the same preexponential even in the compression range, the desorption energies there are about 20–30 % smaller. A more accurate analysis of the data in terms of the desorption parameters is not warranted.

However, a more detailed separate evaluation to obtain abolute desorption energies is not sensible for another reason. As stressed above, the calibration of our temperature scale, which directly enters the energy values, is only as accurate as the literature value of the heat of evaporation of hydrogen (20%). In order to get a reliable energy value to better than this uncertainty, we have therefore resigned ourselves to a different procedure which proceeds in two steps. (i) From the range of pairs of energy/preexponential, we select those for which the preexponential is in the range expected for our system, i.e., about 10^{10} s^{-1} (via detailed balance, the total preexponential is given by the sticking coefficient times the frequency factor; the latter is about 10^{11} s^{-1} as derived from either the dominant vibrations or the value of kT/h; see the discussion in Secs. III C and IV). This results in a desorption energy of about 100 K for ^{4}He, and about 3% less for ^{3}He. (ii) We check this choice by the compatibility of these values with the photodesorption rate which, while independent, also contains the binding energy. A further check is carried out by comparison with theoretical predictions. This will be discussed in Sec. IV.

C. Sticking coefficients

The present experimental apparatus, which has been optimized for TPD starting at very low temperature, is not well suited for sticking measurements. In the desorption configuration, the Pt surface is not fully accessible to a well-defined gas source; in addition, if the cap is cooled in this position, the gas itself does not have a unique thermal distribution because it will scatter off different temperature surfaces before hitting the Pt crystal. On the other hand, if the sample is moved away from this position for dosing to improve this aspect, it sees parts of the apparatus which are at different temperatures, making the effective radiation temperature ill-defined; also, strong influences of photodesorption and collisional desorption arise (both during dosing; the former also during moving and positioning the sample for TPD). However, we do need at least approximate values of the sticking coefficient since sticking enters the desorption rate, via detailed balance, and the interpretation of preexponentials of thermal desorption requires a knowledge of sticking coefficients and their coverage dependence. Therefore, efforts have been made to obtain at least some information on sticking, albeit partly in a semiquantitative and error-prone way.

To accomplish this, the exposure of the surface to helium gas has been done in three different ways.

(i) From the background flux, with the sample moved away from the TPD position. Here, the angular distribution of impinging gas is random. Since the walls are at RT, this is also the gas temperature during dosing, i.e., for the contributions of collisional and photodesorption. The former ends when the dosing is stopped. After that it takes about 70 s to reposition and adjust the sample. Photodesorption proceeds during the entire time and continues during TPD if the Feulner cap is also at RT. However, after 10 s the sample is essentially in position in front of the cap and, if the latter is cooled to 90 K, photodesorption is negligible after this time. These differences allow a semiquantitative estimate of the contributions from these two effects.

(ii) Through a microchannel plate which is at RT and is placed about 3 cm away, parallel to the surface. So the gas is again at RT, but the angular distribution is restricted to about ±20 deg around the surface normal. It takes about 2 min to bring the surface into TPD position after dosing. Here both collisional and photodesorption will be at their maximum.

(iii) The gas reaches the surface through the cap which is cooled to 90 K. In this way, the surface can be left in TPD position during dosing and, if the mass spectrometer filament is switched off during dosing, both collisional and photodesorption are unimportant. There is a further advantage deriving here from the facts that both the time necessary to pump down below 10^{-10} mbar after exposure as well as the background pressure after dosing are minimized.

Each of these dosing modes has its advantages and disadvantages. We therefore report on all three. The values for the sticking coefficients were obtained by differentiation of coverage versus dose curves obtained by integration of desorption spectra after exposure of the surface to a certain gas dose. Owing to the numerous uncertainties mentioned, considerable noise is introduced, see Fig. 9. With data smoothing, the approximate coverage dependence relative to saturation coverage can be extracted, see Fig. 10. The absolute numbers require the knowledge of both the absolute coverage at saturation and of the absolute doses. There is a number of unknowns and uncertainties contained in the determination of the dose. In mode (i), the only quantity not well known is the ion gauge sensitivity, which might introduce an error of 20% in the absolute values. This advantage, however, is far offset by the strong influences of collisional and photodesorption which cannot be clearly separated and quantified reliably. For mode (ii), a calibration of the dose has

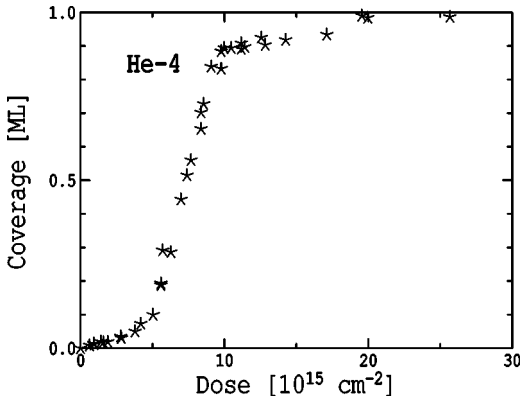

FIG. 9. Adsorption curve (coverage vs exposure) for ^{4}He at $T_s = 2.3$ K and $T_r = 300$ K, obtained from TPD integrals. Dosing method (i).

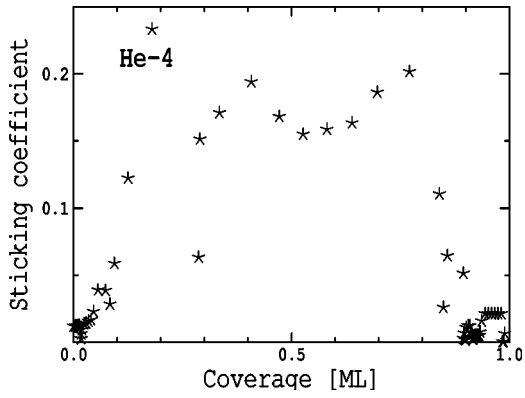

FIG. 10. Sticking coefficient vs coverage derived from the data of Fig. 9.

been done by comparison with neon, for which the sticking coefficient is known[10]; again, collisional and photodesorption have strong influences. Mode (iii) is clearly best defined: both collisional and photodesorption are essentially negligible there, and the dose can be calculated if thermal equilibration of the gas in the cap can be assumed (see Ref. 21 for details). As a result, the values are estimated to be accurate to about ±30%. The following conclusions are drawn.

(i) For 90 K gas, the sticking coefficient at zero coverage, S_0, is about 0.03 for ^{4}He, and also for ^{3}He, because any isotope effect (proportionality to $\sqrt{m_3/m_4}$) is within the experimental uncertainty.

(ii) For 300 K gas, S_0 is about a factor of 10 smaller. For conditions where small impact angles are eliminated [microchannel-plate dosing, (ii)], S_0 is somewhat larger, but due to the uncertainties associated with collisional desorption, this effect cannot be quantified reliably.

(iii) In all cases, S increases with coverage in a sublinear way, reaches a flat maximum around 0.3–0.5 of saturation, and then decreases slowly. The increase with coverage can be understood from the well-known effect of improved coupling of colliding atoms when they impinge on an adsorbate with equal mass and soft vibrations.[8,12,26] The decrease at high coverage, towards zero at saturation, reflects the fact that formation of a second layer is unlikely, in contrast to heavier rare gases.[27,28]

D. Experimental summary

To summarize, the following qualitative picture is the starting point of our detailed analysis with the help of theoretical models. Above 2.3 K, He can exist as a monolayer on Pt(111) and there are two independent mechanisms of desorption occurring around 4 K: thermal desorption and photodesorption.

Thermal desorption shows that, up to a relative coverage of about 0.7 of saturation, He monolayers on Pt(111) behave like (almost) ideal 2D gases. The desorption energies do not vary significantly over this range within our error bars. For ^{4}He, this desorption energy is about 100 K, if combined with "normal" preexponentials of about 10^{10} s^{-1}. If we assume roughly equal preexponentials of desorption for the two isotopes (which is corroborated by the similar appearance of the desorption peaks, with only a small shift), then the difference of peak temperatures of about 0.2 K translates into a desorption energy of ^{3}He, which is about 3% smaller than that of ^{4}He. At coverages above about 0.7 of saturation, a second phase develops which is characterized by continuous desorption through thermal expansion, and a superimposed peak which occurs as this phase disappears as the coverage decreases. Apart from the contribution of zero phonon scattering in sticking, which also shows up in desorption through detailed balance, the only quantum effect observed is due to the difference in zero-point energy. There is no hint of any quantum effects due to the different statistics of the isotopes in the thermal properties of these He (sub)monolayers at our temperatures (2.3 K and up).

The photodesorption is clearly due to direct absorption of photons, not to a (transient) heating effect. It is almost temperature-independent in the range below thermal desorption and close to first order. At a surround temperature of about 300 K it is very noticeable, with a first-order rate constant of about 0.01 s^{-1} for ^{4}He, and about 50% higher for ^{3}He. The dependence on radiation temperature is roughly linear; at 90 K it is four to six times smaller for the two isotopes. The isotope effect shows that it is not desorption due to nonequilibrium phonons.

IV. THEORY AND DETAILED ANALYSIS

A. General formulation

Theory must account for photon-mediated and thermal (phonon-mediated) adsorption and desorption dynamics and kinetics. The task is simplified by the fact that the helium adsorbate is highly mobile (see above) and can therefore be assumed to be in diffusive quasiequilibrium. Thus the time evolution of the adsorbate can be described in terms of macroscopic variables, i.e., coverage, θ, and substrate and radiation temperatures. Because the two kinetic channels are independent of each other, we have

$$\frac{d\theta}{dt} = R_{ad}^{(thermal)} - R_{des}^{(thermal)} + R_{ad}^{(photo)} - R_{des}^{(photo)}. \qquad (1)$$

The phonon-mediated adsorption rate is proportional to the particle flux onto the substrate,

$$R_{ad}^{(thermal)} = S^{(t)}(\theta,T)\frac{P\lambda_{th}a_s}{h}, \tag{2}$$

where $\lambda_{th}=h/\sqrt{2\pi m k_B T}$ is the thermal wavelength of helium atoms in the gas phase at pressure P, a_s is the unit cell area on Pt(111), and T is the common temperature of the adsorbing gas and substrate. The sticking coefficient (probability) is a measure of the energy transfer to the solid via emission of phonons and can be calculated from first principles,[1] or taken from experiment, scaled to the appropriate conditions (see above). An identical expression holds for photon-mediated adsorption for which its sticking coefficient, $S^{(p)}(\theta,T)$, accounts for the probability that a photon is emitted during the collision of the helium atom with the surface.

The thermal desorption rate is given by[14] ($\beta=1/k_BT$)

$$R_{des}^{(thermal)} = S^{(t)}(\theta,T)\frac{a_s}{\lambda_{th}^2}\frac{k_BT}{h}\exp[\beta\mu_{ad}], \tag{3}$$

where $\mu_{ad}(\theta,T)$ is the chemical potential of the adsorbate. This can be written for transparency as

$$\mu_{ad} = -V_0 - k_BT\ln(q_{xy}q_z/\theta) + \mu_{lat}, \tag{4}$$

where μ_{lat} accounts for the lateral He—He interactions in the adsorbate. V_0 is the depth of the adsorption potential for a single helium atom, and

$$q_z = \frac{\exp[\beta h\nu_z/2]}{\exp[\beta h\nu_z]-1}, \tag{5}$$

where ν_z is the frequency of the vibration of a helium atom perpendicular to the surface. At the low temperatures of helium adsorption, and desorption, this simplifies to $q_z \simeq \exp(-\beta h\nu_z/2)$. For a mobile adsorbate with negligible surface corrugation, the partition function for the intraplanar motion is $q_{xy}=a_s/\lambda_{th}^2$. Thus the thermal desorption rate reads

$$R_{des}^{(thermal)} = S^{(t)}(\theta,T)\theta\frac{k_BT}{h}\exp[-\beta(V_0-h\nu_z/2)]\exp[\beta\mu_{lat}]. \tag{6}$$

Detailed balance requires that the desorption rate be proportional to the sticking coefficient, at the temperature of desorption. In the absence of lateral interactions, this rate describes a first-order process, i.e., proportional to θ, for a constant sticking coefficient, with a temperature-dependent rate constant, i.e., the rate for a single atom with a desorption energy which is effectively that required to remove an atom from the lowest bound state of the potential, as shown from first principles for physisorbed systems.[1] In an adsorbate with attractive (repulsive) lateral interactions, μ_{lat} is negative (positive), thus hindering (aiding) desorption.

Photodesorption is caused by the coupling of the electromagnetic field of the impinging thermal radiation into the dynamic dipole of the adsorbate, mediated by a Hamiltonian $H_{em}=-i\hbar(Q/m)\mathbf{A}(\mathbf{x},t)\cdot(\partial/\partial\xi)$. Here $\mathbf{x}$ and ξ are center-of-mass and relative coordinates of the dipole and m is its reduced mass. The effective charge Q is related to the dynamic dipole moment by $\mu_{dyn}=Q[\hbar/(2m\nu_z)]^{1/2}$ with ν_z its resonant frequency. We can envisage two scenarios. (i) The dipole is due to the polarization of the He atom itself, i.e., both positive and negative charges are confined within the volume of the atom apart from its image dipole. Radiation will then excite internal vibrations of this polarization cloud: a resonance phenomenon. To cause desorption, this energy must then be transferred to the center-of-mass motion of the atom via a mechanism similar to that proposed 20 years ago for resonant laser-induced photodesorption of molecules.[15] The intensity of blackbody radiation is not sufficient for that, and the small polarizability of He also makes this very inefficient. (ii) The dipole derives from the charge redistribution in the surface which the adsorbed helium induces and which changes when it moves, as well as the image response to it, i.e., it mainly involves metal electrons. For this scenario, which we adopt here for the photodesorption of helium, we have used density-functional theory for the estimation of polarizabilities, and of static and dynamic dipole moments. Worth noting at this stage is the fact that the dipole moment, and equivalently its effective charge, are decreasing roughly exponentially with increasing distance of the helium atoms from the metal surface, essentially due to the decreasing electronic overlap and interaction.

The photodesorption rate constant (for a single helium atom) is given by[15,16]

$$r_p(T,T_r) = \sum_{i,\mathbf{q}}\frac{2\pi}{\hbar}\sum_{\beta}\int d\mathbf{k}\Omega_{\mathbf{k}}^{-1}|\mathbf{M}_{\mathbf{q},i}\cdot\mathbf{U}_{\mathbf{k}\beta}(0)|^2[n_{\mathbf{k}\beta}\delta(E_{\mathbf{q}}-E_i - \hbar\Omega_{\mathbf{k}}) + (n_{\mathbf{k}\beta}+1)\delta(E_{\mathbf{q}}-E_i+\hbar\Omega_{\mathbf{k}})]P_i. \tag{7}$$

Here

$$P_i = \exp[-E_i/k_BT]\Big/\sum_j \exp[-E_j/k_BT] \tag{8}$$

is the thermal occupation probability of the bound states of helium in the surface potential. The sum over $\mathbf{q}$ runs over the atomic continuum states reached from the bound states via a matrix element

$$\mathbf{M}_{\mathbf{q},i} = i\hbar\frac{Q}{m}\sqrt{\frac{\hbar}{2\varepsilon_0}}\int d\mathbf{x}u_q(\mathbf{x})\frac{\partial}{\partial\mathbf{x}}u_i(\mathbf{x}). \tag{9}$$

$\mathbf{U}_{\mathbf{k}\beta}(0)$ is the field amplitude (of polarization β and wave vector $\mathbf{k}$) at the position of the atom, and $n_{\mathbf{k}\beta}$ is the Bose-Einstein occupation of photons at the radiation temperature T_r.

The photodesorption rate from an adsorbate must also account for the influence of the local environment of the desorbing particle as discussed above, and leads to the coverage dependence of the photodesorption rate being given by

$$R_{des}^{(photo)}(\theta,T,T_r) = r_p(T_r,\theta)\theta\exp[\beta\mu_{lat}]. \tag{10}$$

We have indicated a secondary coverage dependence in the photodesorption rate constant itself because, in principle, the helium atoms already adsorbed will tend to screen the response to the amplitude of the incident electromagnetic field, e.g., by depolarization.

Equating this rate in equilibrium to the photoadsorption rate

$$R_{ad}^{(photo)} = S^{(p)}(\theta, T, T_r)\frac{P\lambda_{th}a_s}{h} = r_p(T_r)\theta\exp[\beta\mu_{lat}] \quad (11)$$

and relating the gas pressure to the chemical potential by

$$P = \frac{k_b T}{\lambda_{th}^3}\exp[\beta\mu_{ad}], \quad (12)$$

we get the photon-mediated sticking coefficient at zero coverage ($\mu_{lat}=0$),

$$S_0^{(p)} = \frac{h}{k_B T}r_p(T_r, \theta = 0). \quad (13)$$

It is important to note that this sticking probability is much smaller than phonon-mediated sticking by many orders of magnitude.

B. Theoretical results: Thermal desorption

To evaluate the desorption rates, we must specify a small number of parameters and the coverage and temperature dependences of the chemical potential of the adsorbate and of the sticking coefficient.

Estimates of the depth of the surface potential, V_0, and the vibrational frequency, ν_z, for ^{4}He on Pt(111) are about 10 meV (Ref. 29) and, on Au(111), 10^{12} s^{-1},[30] respectively. To get a consistent picture, we have done calculations of helium adsorption on jellium using density-functional theory in the local-density approximation.[31,32] We get, respectively, 16 meV and $(2-4)\times 10^{12}$ s^{-1}; this gives a desorption energy between 8 and 11 meV, which agrees with the range of experimental values determined here (see above). We will fine-tune this number when we fit the TPD spectra at low initial coverage. We have fitted the calculated potential energy curve by a Morse potential and find its minimum at $z_0 = 3.2$ Å above the top lattice plane and a range parameter of the order 1 Å.

The facts that (i) He is not localized on sites on the Pt surface and (ii) there is a compressional phase excludes the lattice gas as a model. We allow for some weak attractions between the atoms with a van der Waals–type mean-field model of a two-dimensional gas for which we choose, below the compression range, a contribution, $V\theta$, to the chemical potential.[33] As compression sets in, two responses of the adsorbate are possible: (i) the adsorbate undergoes a transition to a solid phase[34]; (ii) excitations into a "second layer" occur. Both mechanisms would lead to an abrupt lowering in the slope of the chemical potential versus coverage due to crossing of the chemical potentials of the two phases, rather than to a constant chemical potential. Such inflections in the chemical potential as a function of coverage are clearly seen for ^{4}He on graphite,[35] and also emerge from calculations of multilayer formation of both isotopes of helium on a flat surface,[36–38] see in particular Figs. 7 and 10 in Sommer *et al.*[38] For helium adsorption on a metal, the formation of a second layer, some 3 Å above the first layer and bound overwhelmingly by the He—He interaction, is not possible at these temperatures. A more likely structural change is that after the compression of a planar layer has progressed, a further loss of energy due to compression is avoided by excitation into a locally deformed buckled layer. This is most likely due to excitations into the vibrationally excited states of the effective surface potential for which the atoms are further out from the surface (see, e.g., Fig. 2.22 in Kreuzer and Gortel[1]). This would generate a contribution to the chemical potential roughly linear in the number of "buckled" atoms. However, the buckling will be dynamic since the atoms in the ground and the vibrationally excited states will readily interchange their roles.

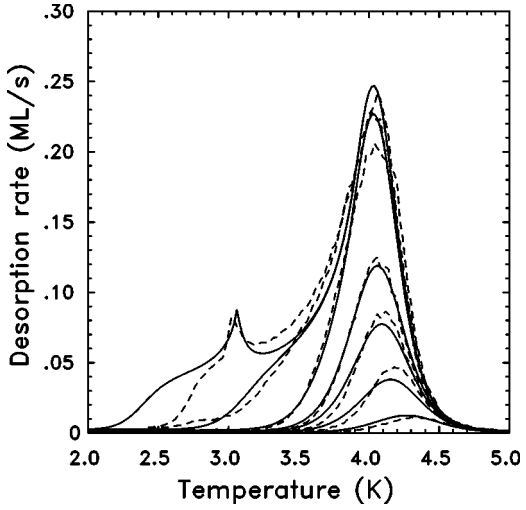

FIG. 11. Comparison of the experimental (dashed curves) and the calculated (solid) TPD rates for ^{3}He for the conditions of Fig. 5. Model parameters: $V_0/k_B=126$, $\nu_z=1.15\times10^{12}$ s^{-1}, $S_0=0.03$, $S_{\max}=0.5$, $V/k_B=-0.6$ K, $r_p=0.0036$ s^{-1}, heating rate 0.2 K s^{-1}. Initial coverages: 0.04, 0.11, 0.22, 0.32, 0.57, 0.76, and 0.95 ML.

To calculate the thermal desorption rate, we also need the sticking coefficient at desorption temperatures. To estimate its zero coverage value around 4 K, we use the forced oscillator model,[12] which worked very well for the heavier rare gases, Ne through Xe. A set of parameters which reproduces our experimental values for gas temperatures 90 K and 300 K leads to an estimate $S_0=0.03$ at 4 K (for a detailed discussion, see Ref. 39). The efficient energy transfer by He—He collisions, as it occurs at increasing coverage, should be much less influenced by temperature. We estimate that, at its maximum, S is 10 to 20 times its initial value. We parametrize the experimental coverage dependence of the sticking coefficient by a simple analytical form

$$S^{(t)}(\theta, T) = S_0^{(t)} + S_{\max}[4\theta(1-\theta)]^{3/4}. \quad (14)$$

Thus we can fit the thermal desorption spectra in the low coverage regime and at low radiation temperature where photodesorption is negligible. With some adjustment of the desorption energy, we get the spectra given in Fig. 11 for ^{3}He for initial coverages below about 1/2 ML. Note that at very low coverages, the peaks in the thermal desorption shift to slightly lower temperatures for increasing coverages. This is explained by the strong increase of sticking with coverage at

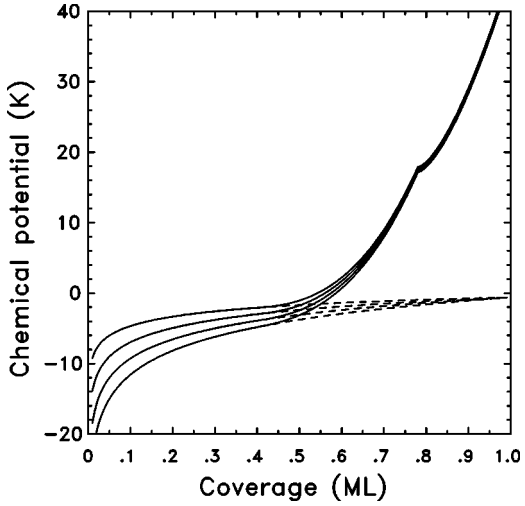

FIG. 12. Chemical potential of a helium adatom, relative to its binding energy, $\mu_{ad}+V_0-h\nu_z/2$, as a function of coverage with (full lines) and without (dashed) higher-order terms added to account for the adlayer compression, at $T=2$, 3, 4, and 5 K (top to bottom).

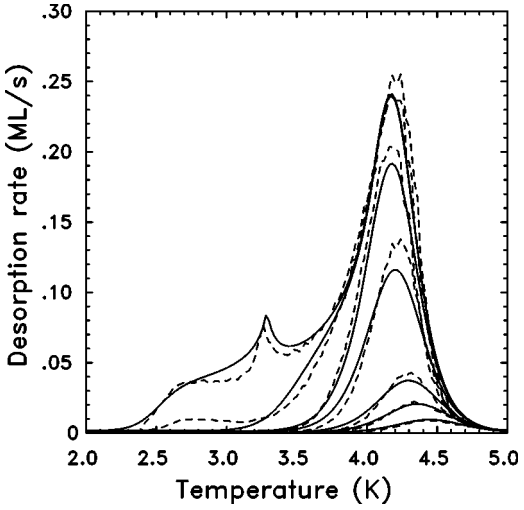

FIG. 13. Comparison of the experimental (dashed curves) and the calculated (solid) TPD rates for ^{4}He. Parameters as for ^{3}He (Fig. 11), except for the mass change, $\nu_z=10^{12}$ s^{-1}. Initial coverages: 0.03, 0.06, 0.11, 0.32, 0.49, 0.70, and 0.94 ML.

low to intermediate coverages (see Fig. 10) with the result that the prefactor in Eq. (6) also increases, enhancing desorption at earlier times as initial coverages are increased. As the sticking coefficient levels off, there is no further downward shift. At this stage any attraction should shift the peaks to higher temperatures. That this is not visible in the data indicates that the attraction is very weak. We estimate that the effective lateral attraction, V, between helium in a relaxed monolayer is less than −1 K. Allowing for coordination, this attraction is more than an order of magnitude smaller than that in the gas phase and consistent with theoretical estimates for 2D He on various substrates.[34,40] The decrease from gas to surface is also consistent with a dipolar He—He repulsion on the metal surface which, using the calculated dipole moment given below, is of order 1 meV (or 10 K) in a monolayer. A critical temperature of less than 1 K, below which a mobile adsorbate on a flat surface would undergo phase separation, results.

For initial coverages larger than about 0.5 ML, we must account for the structural compression to reproduce the low-temperature shoulders and peaks. Following the discussion above, we do this by adding terms to the chemical potential, quadratic and cubic in coverage as pictured in Fig. 12, and adjusted to fit the data. The resulting fit to the TPD spectra for all initial coverages is also given in Fig. 11. Although this procedure is purely phenomenological and detailed calculations of the buckling excitations should be done, it points to the intricate connection between the nature of the inflection in the chemical potential and the shape and position of the compressional peak in TPD. An additional complication is the fact that the sticking coefficient is also affected by the effective repulsion in the compressional region. Such effects of adlayer compression on the chemical potential and the desorption kinetics have been investigated recently for Ar/Pt(111).[41]

With the parameters deduced for ^{3}He, we calculate the TPD spectra for ^{4}He by only changing ν_z by $(4/3)^{1/2}$, which shifts the peaks up in temperature by about 0.2 K and leads to good agreement also for the ^{4}He curves, Fig. 13.

To confirm that the zero-point energy difference is the only quantum effect (apart from that operative in sticking due to the finite probability of zero-phonon scattering) operative under our conditions we have also calculated the desorption spectra treating the adsorbates as a weakly interacting quantum gas. Bose (Fermi) statistics imply effective attractions (repulsions) which result in opposite shifts in desorption spectra for the two statistics. These are not observed experimentally and will become important only at lower temperatures.

C. Theoretical results: adding photodesorption

To evaluate the photodesorption rate, we need the bound states of the surface potential and the dynamic dipole of helium adsorbed on Pt(111). For a Morse potential, the bound and continuum state energies and wave functions are known analytically; relevant quantities are listed in the Appendix. The population factor (8) ensures that the contribution of the excited states to the rate is negligible for our surface potential and a substrate temperature of a few degrees Kelvin.

From the density-functional calculations, we can estimate the dipole moment and hence the effective charge. The z dependence of the dipole moment is roughly represented by

$$\mu(z) = \mu_0 \exp[-(z-z_0)/z_c] \tag{15}$$

with z_c roughly (0.2–0.4) Å and the permanent dipole moment $\mu_0 \approx 0.005\ e$Å; we also get the atomic polarizabilities $\alpha_0 \approx 0.23$ Å and $\alpha_v \approx 0.002$ Å^3. This gives a dynamic dipole $\mu_{dyn}=(\alpha_v h\nu_z/2)^{1/2}=0.005\ e$Å. For the effective charge $Q(z)=(\partial\mu/\partial z)/\sqrt{2}$, we thus have $Q(z)=Q_0\exp[-(z-z_0)/z_c]$ (Ref. 42) with an effective charge $Q_0 \approx 0.01e$.

To illustrate the essential dependence of the photodesorption rate constant on the mass, radiation temperature, and charge (or dynamical dipole moment), we take, in Eq. (9), a

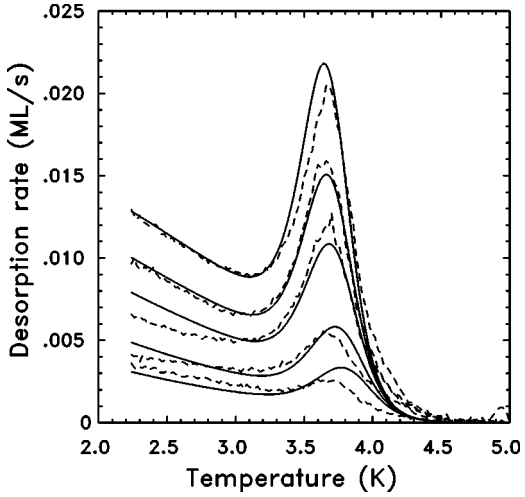

FIG. 14. Comparison of experimental (dashed lines) and calculated TPD spectra for ^{3}He at a radiation temperature of 290 K. Thermal desorption parameters as in Fig. 11, except heating rate of 0.03 K s^{-1}. Initial coverages: 0.15, 0.24, 0.41, 0.54, and 0.72 ML.

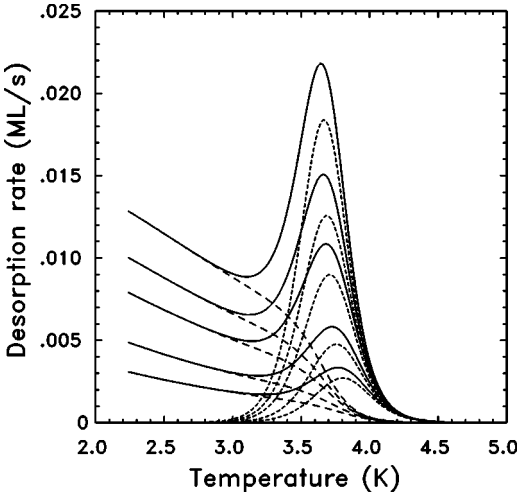

FIG. 15. Model curves of Fig. 14 showing the separate contributions of photodesorption (dashed lines) and thermal desorption (dotted lines).

Gaussian of range z_g (related to the zero-point energy) for the lowest bound state wave function, $u_0(z)$, and plane waves for the continuum states. The resulting rate can be simplified to

$$r_p = \frac{16\pi^{1/2}Q_0^2}{3\varepsilon_0 mhc^3} k_B T_r \nu_z \exp[(z_g/z_c)^2] \times \int_0^\infty dx[x^2 + (z_g/z_c)^2] \frac{(ax^2+b)\exp[-x^2]}{\exp[ax^2+b]-1}, \quad (16)$$

where $x=|\mathbf{q}|z_g$, $a=h\nu_z/2k_BT_r$, and $b=(V_0/k_BT_r-a)$.

We have evaluated the rate constant r_p for the potential parameters of Figs. 11 and 13. In the range from 50 to 300 K it rises somewhat faster than linear with the radiation temperature, by about an order of magnitude. If the frequency ν_z (on a different substrate) is lower by at least an order of magnitude, then this rise would be quite close to linear. As for the mass dependence, we note that z_c and z_g scale with ν_z in roughly the same way so that the photodesorption rate scales roughly like $m^{-3/2}$, i.e., according to the prefactor alone because, for small enough a, the terms involving b dominate the integral and vary little with mass. At 300 K, typical values are $r_p/Q_0^2 \approx 20$, 3.0, and 0.3 for $\nu_z = 10^{13}$, 10^{12}, and 10^{11} s^{-1} and $z_c = z_g$. Neglecting the z dependence of the effective charge ($z_c \to \infty$) reduces these rates by a factor of about 10. Clearly, Eq. (16) implies that the rate constant is a sensitive function of the ratio z_g/z_c.

The comparison with the experimental photodesorption contributions is based on the matrix elements calculated for a Morse potential and not on the simplified result (16), see the Appendix. With the potential parameters obtained from the analysis of thermal desorption data, we have essentially determined all parameters entering the photodesorption rate as well.

To obtain a good fit to the data, we need some adjustment to Q_0 and to the lateral interaction V. The former controls the magnitude of the photodesorption rate constant; for the smaller estimate of the ratio $z_g/z_c \simeq 2.5$, we find that $Q_0 \approx 0.008e$. The lateral interaction controls the coverage dependence of the photodesorption rate. We recall that the thermal desorption peaks indicate a rather weak, albeit almost negligible lateral attraction. However, at the lowest measuring temperature, the rate is fortunately sensitive to the lateral interaction and thus allows a more precisely determination; we obtain $V/k_B = -0.6$ K to fit the initial rates for initial coverages below the onset of compression for ^{3}He, and a radiation temperature of 290 K. The complete desorption traces are then generated without further parameter adjustments, i.e., with the thermal contribution obtained as in Fig. 11 but for a change of heating rate. These are shown in Fig. 14; a breakdown of the two contributions is shown in Fig. 15.

Unlike the spectra for 90 K radiation in which the effect of structural compression was visible for coverages above 0.5 ML, here the effect is not apparent in this coverage range, even for the fastest heating rate (0.2 K/s). The absence of compression effects in this regime where photodesorption dominates can be explained with the assumption that the photodesorption process is largely unaffected by the compression. Incorporating this feature into our model, we are able to reproduce the corresponding experimental traces in Fig. 14, as well as the spectra obtained for higher heating rates with a cap temperature of 290 K (not exhibited).

There is a straightforward justification for this assumption. The photodesorption rate (11) has a coverage dependence which involves a product of a sticking coefficient for photoadsorption and an activity factor which includes compressional effects. The latter increases sharply in the compression region, e.g., by a factor of 100 at the compression peak in Fig. 11, implying a corresponding increase in the photodesorption rate. Even for lower coverages, a significant increase in the photodesorption rate would be expected if the sticking coefficient for photoadsorption was unaffected by the compression, i.e., constant for coverages above 0.5 ML. Theory would then predict initial rates, around 2.5 K in Fig. 14, well above 0.02 ML/s. This would desorb a noticeable fraction of a monolayer within a few tenths of a degree, with

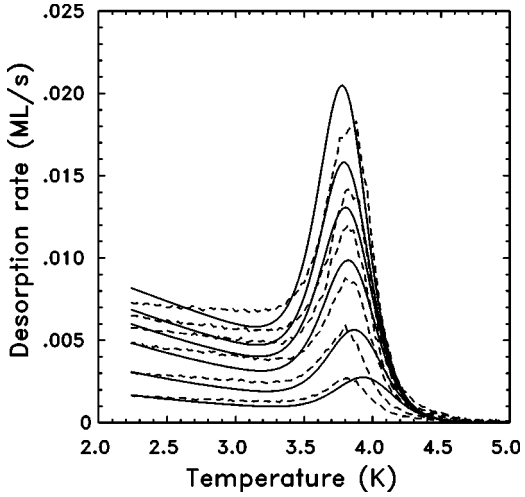

FIG. 16. Same as Fig. 14 but for ^{4}He and initial coverages 0.12, 0.24, 0.38, 0.49, 0.57, and 0.71 ML.

initially distinct desorption traces overlaying each other, once their coverages fell below the compression region. As this is not observed, a compensating effect in the desorption rate must exist, which can only come from the sticking coefficient. This is to be expected because, at the onset of compression, the bare metal surface which mediates the photoabsorption process has disappeared, i.e., the sticking coefficient for the process has to decrease, and by a similar magnitude.

As to the isotope effect, r_p varies like $m^{-3/2}$ in agreement with experiment. The result is to decrease the photodesorption rate for ^{4}He and, with no further adjustment, the theory produces the rates shown in Fig. 16. The isotope effect is visible by comparison to Fig. 14. The initial desorption rate for the high heating rate data and 90 K environment, Fig. 11, is well fitted by reducing R_{photon} by a factor 6, consistent with our theoretical estimate. The agreement between theory and experiment is excellent in all aspects considering the simplicity of the model and the remaining uncertainties in the experimental data.

Inspection of the integrand of the photodesorption rate constant reveals that the He atoms desorb in a narrow range of kinetic energies centered around the zero-point energy of the adatom, because the transition probability from bound to continuum states of He is a convolution of the continuum density of states (rising with energy) and the blackbody spectrum (dropping sharply at high energy). The close-to-linear dependence on the radiation temperature, mentioned above, is essentially due to the narrowness of this distribution.

Finally, we discuss the question of quantum efficiency. The overall quantum efficiency of the photodesorption process, defined as the ratio of the photodesorption rate constant to the flux of incoming photons (of all energies) per unit cell of area a_s, is given by

$$\eta = \frac{r_p(T_r)}{a_s \sigma T_r^3 / k_B}, \tag{17}$$

where σ is the Stefan-Boltzmann constant. Another definition would involve energy rather than particle fluxes, in which case we multiply the numerator by the average energy of desorption and the denominator by $k_B T_r$. In either case we find quantum efficiencies of order 10^{-6} at $T_r = 300$ K and smaller by a factor of 6 at 90 K.

V. SUMMARY

To summarize, in the first investigation of adsorption/desorption kinetics of ^{4}He and ^{3}He on a macroscopic single-crystal surface, Pt(111), which we have used to extract adsorption and desorption parameters, we have also found a quantum effect, photodesorption by far-infrared photons through direct coupling to the transition dipole induced in the surface by adsorbed helium. The proposed theory can recover the main properties of both the thermal and the photoinduced desorption; for the latter these are its approximate absolute magnitude (with overall efficiency of about 10^{-6} at $T_r = 300$ K) and its dependences on radiation temperature (roughly linear) and on mass (50% higher for He-3 than for He-4).

As expected from earlier work,[1,40] quantum effects are not significant in the main thermal desorption range, as shown by our reproduction of the (very small) isotope effect. The thermal desorption spectra show that the helium submonolayer is an almost ideal two-dimensional gas up to a coverage of about 0.6 of saturation. The desorption energy in this range is about 100 K, with normal preexponentials of about 10^{10} s^{-1}–10^{11} s^{-1} depending on the value of the coverage-dependent sticking coefficient. Above this coverage, a compression phase is formed which might be understandable in terms of a dynamically buckled layer. The coverage dependence of the effective preexponential is influenced by that of the thermal sticking coefficient. The latter is about 0.03 on the bare surface at 2.3 K; it increases with coverage in the low coverage range and decreases strongly in the compression range.

ACKNOWLEDGMENTS

We thank Wolfgang Friess for performing the forced oscillator calculations of sticking, and Peter Feulner for valuable discussions. The work in Munich was supported by the Deutsche Forschungsgemeinschaft through SFB 338, TP C11, and by the Fonds der Chemischen Industrie. The work at Dalhousie University was supported by grants from the Office of Naval Research and by the Natural Sciences and Engineering Research Council of Canada.

APPENDIX

In this appendix, we comment on the matrix element (9) and give a result for the photodesorption rate in the dipole approximation. The surface dipole moment of an adsorbed particle can be shown on the basis of quantum-mechanical calculations to be a decreasing function of distance from the surface. The effective charge Q in this matrix element must reflect this dependence so that Eq. (9) becomes

$$\mathbf{M}_{\mathbf{q},i} = i\frac{\hbar}{m}\sqrt{\frac{\hbar}{2\varepsilon_0}}\int d\mathbf{x} Q(\mathbf{x}) u_q(\mathbf{x}) \frac{\partial}{\partial \mathbf{x}} u_i(\mathbf{x}). \tag{A1}$$

Replacing the momentum operator by a commutator of the Hamiltonian and the position operator, we can transform this matrix element to

$$\mathbf{M}_{\mathbf{q},i} = -i\frac{(E_q - E_i)}{\hbar}\sqrt{\frac{\hbar}{2\varepsilon_0}}\int d\mathbf{x} u_q(\mathbf{x})\mu(\mathbf{x})u_i(\mathbf{x}), \quad \text{(A2)}$$

where $\mu(\mathbf{x}) = Q(\mathbf{x})\mathbf{x}$ is the dipole moment operator. This transformation is strictly valid only for a static dipole moment with constant charge in which case it also arises from an interaction $-\mu(\mathbf{x})\cdot\mathbf{E}(\mathbf{x})$ in the Hamiltonian. On the other hand, time-dependent fields are included in the quantum-mechanical Hamiltonian via minimal coupling $-i\hbar[Q(\mathbf{x})/m]\mathbf{A}(\mathbf{x},t)\cdot(\partial/\partial\mathbf{x})$ of the charge to the vector potential from which the matrix element (9) originated.

Approximating the dipole moment obtained in a density-functional calculation by an exponential (15) and using the analytically known wave functions in a Morse potential, we can evaluate the matrix elements and hence the photodesorption rate constant. The potential is

$$V(z) = V_0\{\exp[-2\gamma(z - z_0)] - 2\exp[-\gamma(z - z_0)]\} \quad \text{(A3)}$$

with bound states at

$$E_n = -V_0\left[\frac{\sigma - n - 1/2}{\sigma}\right]^2,$$

$$\sigma^2 = \frac{2mV_0}{\hbar^2\gamma^2}. \quad \text{(A4)}$$

If we match the zero-point energy to that of a harmonic oscillator, $\sigma = V_0/(h\nu_z/2)$, we obtain $\sigma = 5.25$ for the fitted potential parameters of the ^{4}He system, $V_0/k_B = 126$ K and $\nu_z = 10^{12}$ s^{-1}; there are five bound states. The contribution from the lowest bound state to the photodesorption rate constant (7) then reads

$$r_p(T_r) = \frac{2\mu_0^2}{3\pi\varepsilon_0 c^3\hbar^4}(k_B T_r)^3\frac{2\sigma - 1}{(2\sigma)^{2d-1}\Gamma^2(d)\Gamma(2\sigma)} \times \int_0^\infty dx F(\sigma,d;x)\frac{x(ax^2+b)^3}{\exp[ax^2+b]-1}, \quad \text{(A5)}$$

$$F(\sigma,d;x) = \frac{\left|\Gamma\left(\sigma + d - \frac{1}{2} - i\eta\right)\right|^4}{\left|\Gamma\left(\sigma + \frac{1}{2} - i\eta\right)\right|^2}\frac{\sinh(2\pi\eta)}{\cos(2\pi\sigma) + \cosh(2\pi\eta)}, \quad \text{(A6)}$$

where $\eta = |\mathbf{q}|\gamma^{-1} = \pi\sigma^{1/2}x$, $d^{-1} = z_c\gamma$, and a, b are as in Eq. (16). Upon integration, the mass and temperature dependence of this expression are almost identical to that presented in the simplified expression (16); the explicit cubic temperature dependence in Eq. (A5) is reduced to a near-linear one through the dominance of b in the integrand. The alternate expression to Eq. (A5) with Q_0 explicit gives values for the rate constant which agree within 30%, for ranges of parameters, for the corresponding value of μ_0.

[1] H. J. Kreuzer and Z. W. Gortel, *Physisorption Kinetics* (Springer-Verlag, Berlin, 1986).

[2] L. Bruch, M. W. Cole, and E. Zaremba, *Physical Adsorption: Forces and Phenomena* (Oxford University Press, Oxford, 1997).

[3] M. W. Cole, D. R. Frankl, and D. L. Goodstein, Rev. Mod. Phys. **53**, 199 (1981).

[4] M. Weimer, R. M. Housley, and D. L. Goodstein, Phys. Rev. B **36**, 5199 (1987), and references therein.

[5] P. Taborek, Phys. Rev. Lett. **48**, 1737 (1982).

[6] M. Sinvani, D. L. Goodstein, M. W. Cole, and P. Taborek, Phys. Rev. B **30**, 1231 (1984).

[7] D. L. Goodstein, R. Maboudian, F. Scaramuzzi, M. Sinvani, and G. Vidali, Phys. Rev. Lett. **54**, 2034 (1985).

[8] H. Schlichting and D. Menzel, Surf. Sci. 272, (1992); **285**, 209 (1993).

[9] W. Friess, H. Schlichting, and D. Menzel, Phys. Rev. Lett. **74**, 1147 (1995).

[10] W. Friess, Ph.D. thesis, Techn. Univ. Muenchen, 1995.

[11] H. Schlichting, D. Menzel, T. Brunner, W. Brenig, and J. C. Tully, Phys. Rev. Lett. **60**, 2515 (1988).

[12] H. Schlichting, D. Menzel, T. Brunner, and W. Brenig, J. Chem. Phys. **97**, 4453 (1992), and references therein.

[13] W. Widdra *et al.*, Phys. Rev. B **57**, 4111 (1998).

[14] See, e.g., H. J. Kreuzer and S. H. Payne, in *Computional Methods in Surface and Colloid Science*, edited by M. Borowko (Marcel Dekker Inc., New York, 2000).

[15] Z. W. Gortel, H. J. Kreuzer, P. Piercy, and R. Teshima, Phys. Rev. B **27**, 5066 (1983).

[16] P. Piercy, Z. W. Gortel, and H. J. Kreuzer, in *Advances in Multi-Photon Processes and Spectroscopy*, edited by S. H. Lin (World Scientific Publ., Singapore, 1987), Vol. 3, p. 105.

[17] K. A. Pearlstine and G. M. McClelland, Surf. Sci. **134**, 389 (1983).

[18] M. Hassel, K. Svensson, M. Persson, and S. Andersson, Phys. Rev. Lett. **80**, 2481 (1998); M. Hassel, K. Svensson, J. Bellman, S. Andersson, and M. Persson, Phys. Rev. B **65**, 205402 (2002).

[19] T. Niedermayer, H. Schlichting, D. Menzel, S. H. Payne, and H. J. Kreuzer, Phys. Rev. Lett. **89**, 126101 (2002).

[20] H. Schlichting and D. Menzel, Rev. Sci. Instrum. **64**, 2013 (1993).

[21] T. Niedermayer, Ph.D. thesis, TU München (2002).

[22] The sample cools from 1000 K to about 500 K in about 3 min in the disconnected state. Then the cryostat head is connected, whereupon the sample cools to about 40 K in a few seconds. It takes another 6 min to arrive at about 2.3 K.

[23] P. Feulner and D. Menzel, J. Vac. Sci. Technol. **17**, 662 (1980).

[24] The saturation coverage attained at low radiation and gas temperatures has been defined as one monolayer. The maximum coverage obtainable with radiation and dosing gas at RT was 0.65 to 0.85 of that, depending on dosing mode, heating rate, and time elapsed between dosing and measurement.

[25] T. Niedermayer, H. Schlichting, and D. Menzel (unpublished).
[26] M. Head-Gordon, J. C. Tully, H. Schlichting, and D. Menzel, J. Chem. Phys. **95**, 9266 (1991).
[27] P. Zeppenfeld, J. Goerge, M. Buechel, R. David, and G. Comsa, Surf. Sci. Lett. **318**, L1187 (1994).
[28] H. J. Kreuzer, Surf. Sci. Lett. **344**, L1264 (1995).
[29] K. T. Tang and J. P. Toennies, Surf. Sci. Lett. **279**, L203 (1992).
[30] E. Zaremba and W. Kohn, Phys. Rev. B **15**, 1769 (1977).
[31] N. D. Lang and W. Kohn, Phys. Rev. B **1**, 4555 (1970); **3**, 1215 (1971); **7**, 3541 (1973).
[32] Although the applicability of density-functional theory is questionable for the energetics of physisorption, its use (later) for calculating the field-induced dipole moment and effective charge is more sound. We report all our parameters.
[33] For small coverages, this is equivalent to the Bragg-Williams approximation of the lattice gas.
[34] P. A. Whitlock, G. V. Chester, and M. H. Kalos, Phys. Rev. B **38**, 2418 (1988); M. E. Pierce and E. Manousakis, *ibid.* **62**, 5228 (2000).
[35] R. E. Elgin and D. L. Goodstein, Phys. Rev. A **9**, 2657 (1974).
[36] P. Summerside, E. Sommer, R. Teshima, and H. J. Kreuzer, Phys. Rev. B **25**, 6235 (1982).
[37] E. Sommer and H. J. Kreuzer, Phys. Rev. B **26**, 658 (1982).
[38] E. Sommer and H. J. Kreuzer, Phys. Rev. B **26**, 4094 (1982).
[39] W. Friess and D. Menzel (unpublished).
[40] R. L. Siddon and M. Schick, Phys. Rev. A **9**, 907 (1974); A. D. Novaco and C. E. Campbell, Phys. Rev. B **11**, 2525 (1975).
[41] G. A. Kimmel, M. Persson, Z. Dohnalek, and B. D. Kay, J. Chem. Phys. **119**, 6776 (2003).
[42] The *z* dependence was omitted in our Letter (Ref. 19), which led to an overestimate of the effective charge.